Behavioral/Cognitive

Gyral Crowns Contribute to the Cortical Infrastructure of Human Face Processing

Ethan H. Willbrand,[1,2] Joseph P. Kelly,[3] Xiayu Chen,[4] Zonglei Zhen,[4,5] Guo Jiahui,[6] Brad Duchaine,[7] and Kevin S. Weiner[8,9,10]

[1]Medical Scientist Training Program, School of Medicine and Public Health, University of Wisconsin–Madison, Madison, Wisconsin 53705, [2]Department of Radiology, University of Wisconsin School of Medicine and Public Health, Madison, Wisconsin 53792, [3]Department of Psychiatry and Behavioral Sciences, Feinberg School of Medicine, Northwestern University, Chicago, Illinois 60611, [4]Faculty of Psychology, Beijing Normal University, Beijing 100875, China, [5]State Key Laboratory of Cognitive Neuroscience and Learning, Beijing Normal University, Beijing 100875, China, [6]School of Behavioral and Brain Sciences, The University of Texas at Dallas, Richardson, Texas 75080, [7]Department of Psychological and Brain Sciences, Dartmouth College, Hanover, New Hampshire 03755, [8]Helen Wills Neuroscience Institute, University of California Berkeley, Berkeley, California 94720, and Departments of [9]Psychology and [10]Neuroscience, University of California Berkeley, Berkeley, California 94720

Neuroanatomical features across spatial scales contribute to functional specialization and individual differences in behavior across species. Among species with gyrencephalic brains, gyral crown height, which measures a key aspect of the morphology of cortical folding, may represent an anatomical characteristic that importantly shapes neural function. Nevertheless, little is known about the relationship between functional selectivity and gyral crowns—especially in clinical populations. Here, we investigated this relationship and found that the size and gyral crown height of the middle, but not posterior, face-selective region on the fusiform gyrus were decreased in individuals with developmental prosopagnosia ($N = 22$; 68% female; aged 25–62) compared with neurotypical controls (NTs; $N = 25$; 60% females; aged 21–55), and this difference was related to face perception. Additional analyses replicated the relationship between gyral crowns and face-selective region size in 1,053 NTs (55% females; aged 22–36). These results inform theoretical models of face processing while also providing a novel neuroanatomical feature contributing to the cortical infrastructure supporting face processing.

Key words: **cortical folding; developmental prosopagnosia; face processing; fusiform face area; fusiform gyrus; neuroimaging**

Significance Statement

Understanding how brain structure supports specialized brain functions is a central goal of neuroscience. Here, we identified a role of gyral crown height—an understudied cortical feature—in shaping the cortical infrastructure underlying face processing. By examining face-selective regions of the fusiform gyrus in both neurotypical individuals and those with developmental prosopagnosia, we demonstrate that reduced gyral crown height is associated with a diminished face-selective region surface area and impaired face recognition ability. Furthermore, this structural–functional relationship extends to a large neurotypical sample of over 1,000 individuals, highlighting a generalizable link between cortical anatomy and functional specialization. These findings introduce a new neuroanatomical factor to theoretical models of face perception, which could extend to additional neurodevelopmental disorders and other cognitive tasks.

Received March 20, 2025; revised Aug. 26, 2025; accepted Oct. 21, 2025.

Author contributions: E.H.W. and K.S.W. designed research; E.H.W., J.P.K., X.C., Z.Z., and K.S.W. performed research; X.C., Z.Z., G.J., and B.D. contributed unpublished reagents/analytic tools; E.H.W., J.P.K., X.C., Z.Z., G.J., and K.S.W. analyzed data; E.H.W. and K.S.W. wrote the paper.

This research was supported by NSF CAREER Award 2042251 (K.S.W.), NIH Medical Scientist Training Program Grant T32 GM140935 (E.H.W.), NIH T32 NS047987 (J.P.K.), NSF GRFP Award DGE-2234667 (J.P.K.), as well as a Key Program of National Natural Science Foundation of China 62236001 (Z.Z.) and a General Program of National Natural Science Foundation of China 31771251 (Z.Z.). Data collection at Dartmouth was supported by a Rockefeller Foundation award. We thank Guo Jiahui and Hua Yang for their work with recruitment and data collection for the original project and the participants for participating.

The authors declare no competing financial interests.

Correspondence should be addressed to Kevin S. Weiner at kweiner@berkeley.edu.

https://doi.org/10.1523/JNEUROSCI.0562-25.2025

Introduction

Charting the relationship among brain structure, brain function, and behavior, as well as how these relationships differ in neurodevelopmental disorders, are primary goals in neuroscience. Developmental prosopagnosia (DP) is an intriguing neurodevelopmental disorder to investigate these relationships as individuals with DP have profound deficits in face recognition despite normal low-level vision, normal intelligence, and no explicit insult to the brain (Susilo and Duchaine, 2013; Behrmann et al., 2016). Broadly speaking, the fusiform face area (FFA; Kanwisher et al., 1997; Kanwisher, 2010), which is a widely studied functional region on the lateral fusiform gyrus (FG) that is

causally involved in face perception (Parvizi et al., 2012; Rangarajan et al., 2014; Duchaine and Yovel, 2015; Schalk et al., 2017; Jonas et al., 2018; Jonas and Rossion, 2021), is often a functional neuroanatomical target in DP studies.

However, ongoing research shows that there are at least two functionally and structurally distinct face-selective regions on the FG in neurotypical controls (NTs; Pinsk et al., 2009; Weiner et al., 2010, 2014, 2016, 2017a; Weiner and Grill-Spector, 2010; Davidenko et al., 2012; Julian et al., 2012; Kietzmann et al., 2012; Parvizi et al., 2012; Çukur et al., 2013; Engell and McCarthy, 2013; McGugin et al., 2014, 2015, 2016; Gomez et al., 2015, 2017, 2018; Kay et al., 2015; Stigliani et al., 2015, 2019; Zhen et al., 2015; Natu et al., 2016, 2019; Elbich and Scherf, 2017; Scherf et al., 2017; Rosenke et al., 2020, 2021; Finzi et al., 2021; Nordt et al., 2021; Chen et al., 2023; Weiner and Willbrand, 2023). Indeed, one such study recently showed that two FG face-selective regions—pFus-faces/FFA-1 and mFus-faces/FFA-2—were distinct based on architectural, functional, and connectivity features in over 1,000 participants (Chen et al., 2023). Despite numerous studies in NTs, to our knowledge, no study has tested the structural, functional, and behavioral relevance of these distinct FG face-selective regions in DPs and NTs.

To fill this gap in knowledge, we first manually identified FG face-selective regions in 47 participants (22 DPs and 25 NTs) to determine whether the incidence rates of FG face-selective regions differed between groups. Second, using prior criteria (Chen et al., 2023), we assessed whether the topographical patterning of the FG face-selective regions differed between groups. Third, we extracted neuroanatomical and morphological features (gyral height, cortical thickness, surface area) of each region and tested for group-related differences. We targeted gyral height as recent research showed a relationship between genetics and cortical curvature (gyral crowns in face-selective regions and sulcal pits in place-selective regions) in ventral temporal cortex (VTC; Abbasi et al., 2020), and this feature is understudied compared with many other folding features such as depth, width, and gray matter thickness (e.g., Im et al., 2010; Alemán-Gómez et al., 2013; Madan, 2019; Willbrand et al., 2023, among others). Fourth, we tested whether neuroanatomical properties correlated with the size of FG face-selective regions. Fifth, we examined whether the extracted properties of the FG face-selective regions were related to individual differences in face perception ability (Duchaine and Nakayama, 2006) and if neuroanatomical properties mediated this relationship. Sixth, we tested whether any structure–function relationships identified in this sample extended to a separate, larger sample from the Human Connectome Project ($N = 1{,}053$; Chen et al., 2023).

This multipronged approach showed that (1) FG face-selective region incidence does not differ between groups; (2) FG face-selective region gyral crown height, but not cortical thickness, was decreased in DPs; (3) mFus-faces/FFA-2, but not pFus-faces/FFA-1, was smaller in DPs; (4) there was a relationship between FG face-selective region gyral crown height and size in both samples; (5) the size of mFus-faces/FFA-2, but not pFus-faces/FFA-1, was positively correlated with face perception ability; and (6) the relationship in (5) was mediated by mFus-faces/FFA-2 gyral crown height. These results inform theoretical models of face processing and provide a novel neuroanatomical feature (gyral crowns) contributing to the cortical infrastructure supporting face processing.

Materials and Methods

Experimental model and subject details

Participants. Dataset 1: Twenty-two DPs (seven males; mean age = 41.9 ± 12.0 years old, 21–55 years old; 17 right-handed) and 25 NTs (10 males; mean age = 42.3 ± 10.1 years old, 25–62 years old; 22 right-handed) participated in the study. Demographics did not differ between groups ($ps > 0.55$). DPs were recruited from www.faceblind.org and all reported problems in daily life with face recognition. DP contacts were not invited to participate if they had an autism spectrum disorder (ASD) diagnosis or suspected they were autistic. To assess their face recognition, we tested DPs with the Cambridge Face Memory Test (CFMT; Duchaine and Nakayama, 2006), a famous face test (Duchaine and Nakayama, 2005), and an old–new face discrimination test (Duchaine and Nakayama, 2005). All but one DP performed two or more standard deviations (SDs) below the mean of published control results in at least two of the three diagnostic tests (Duchaine et al., 2007a,b). The DP participant who did not reach −2 SDs on two tests scored poorly on two of the three tasks (CFMT, $z = -1.9$; famous face, $z = -7.1$; old–new, $z = -0.5$), so we included this single participant to increase the sample size. All participants had normal or corrected-to-normal vision and had no current psychiatric disorders. Participants provided written informed consent before doing the tasks, and all procedures were approved by Dartmouth's Committee for the Protection of Human Participants. Participants were leveraged from a prior study on category selectivity in DP (Jiahui et al., 2018) and on ventral temporal sulcal morphology in DP (Parker et al., 2023).

Dataset 2: Data for the Human Connectome Project (HCP) neurotypical adult cohort analyzed in the present study were sourced from the freely available HCP database (https://humanconnectome.org/study/hcp-young-adult; Van Essen et al., 2012). The dataset consisted of 1,053 participants (575 females; ages 22–36). These data were previously acquired using protocols approved by the Washington University Institutional Review Board.

Method details

Face recognition task. Dataset 1: In the present study, we focused on the CFMT as our quantitative measure of face recognition for three main reasons. First, the CFMT is a commonly used measure of unfamiliar face recognition (Duchaine and Nakayama, 2006). Second, the CFMT is a well-established test with high reliability: previous studies show a Spearman–Brown split-half reliability for CFMT of 0.91, as well as a test–retest reliability of 0.70 and alternate forms of reliability of 0.76 (Wilmer et al., 2010, 2012). Third, we focus on the CFMT to maximize the number of participants included in the present measurements. Specifically, the majority of participants (except one NT) completed the CFMT. Given that face processing deficits are also evident in ASD (Dawson et al., 2005), future work can also test if the relationships identified here extend to individuals with ASD as well as include the Autistic Trait Questionnaire in future brain structure–function studies in DPs (which was not included in the present study).

MRI data. Brain data acquisition. Dataset 1: All participants were scanned in a 3.0 T Philips MRI scanner (Philips Medical Systems) with a SENSE (SENSitivity Encoding) 32-channel head coil. A high-resolution anatomical volume was acquired at the beginning of the scan using a high-resolution 3D magnetization-prepared rapid gradient-echo sequence (220 slices; field of view, 240 mm; acquisition matrix, 256 × 256; voxel size, 1 × 0.94 × 0.94 mm).

Dataset 2: Anatomical T1-weighted MRI scans (0.7, mm voxel resolution) were obtained in native space from the HCP database, along with outputs from the HCP-modified FreeSurfer pipeline (v5.3.0; Dale et al., 1999; Fischl et al., 1999a; Glasser et al., 2013). Additional details on image acquisition parameters and image processing can be found in Glasser et al. (2013). All subsequent sulcal labeling and extraction of anatomical metrics were calculated from the cortical surface reconstructions of individual participants generated through the HCP's custom modified version of the FreeSurfer pipeline (Glasser et al., 2013).

Cortical surface reconstruction. Cortical surface reconstructions were generated for each participant from their T1 scans using the standard

FreeSurfer pipeline (v6.0.0; https://surfer.nmr.mgh.harvard.edu; Dale et al., 1999; Fischl et al., 1999a,b). Cortical reconstructions were created from the resulting boundary made by segmenting the gray and white matter in each anatomical volume with FreeSurfer's automated segmentation tools (Dale et al., 1999). Subsequent region of interest (ROI) labeling and extraction of morphological metrics were calculated from individual participants' cortical surface reconstructions. This process was carried out blind to the participant group.

Functional localizer. *Dataset 1*: A detailed description of the functional scanning parameters has been previously described in Jiahui et al. (2018). Here, we provide a brief overview. Participants completed a one-back task during a dynamic localizer scan containing five visual categories (faces, scenes, bodies, objects, and scrambled objects). Each participant completed five scans, composed of 10 12 s category blocks of video clips interleaved with 12 s fixation blocks (4.2 min in total). Each visual category was displayed twice in each scan in a quasirandom order. In each category block, six 1,500 ms video clips were presented interleaved by blank fixation screens presented for 500 ms. Stimuli were presented using SuperLab 4.5.3 (https://cedrus.com/superlab/index.htm) and displayed to the participant via a Panasonic DT-4000UDLP projector (resolution, 1,024 × 768; refresh rate, 60 Hz) at the rear of the scanner.

The five runs were then divided into localization runs and test runs to carry out a "leave-one-out" analysis (Norman-Haignere et al., 2013, 2016). In each of the leave-one-out combinations, four of the five runs for a participant were used to localize the vertices that showed the strongest preference for the preferred category. To avoid "double-dipping" (Kriegeskorte et al., 2009), the responses of the selected voxels to each stimulus condition were then measured in the left-out run. All five combinations were analyzed and then averaged to produce the final result for each participant. Finally, face-selective maps were created from the difference between the response to faces and the response to objects for each participant.

Dataset 2: Face-selective regions in HCP participants were localized using a working memory task in which four stimulus types (faces, places, tools, and body parts) were presented in separate blocks (Barch et al., 2013). The localizer consisted of two runs, and each run contained eight task blocks (10 trials of 2.5 s each, for 25 s) and four fixation blocks (15 s each). Within each run, half of the task blocks used a two-back working memory task and the other half implemented a zero-back working memory task. A 2.5 s cue indicated the task type at the start of the block. For each trial, the stimulus was presented for 2 s, followed by a 500 ms intertrial interval. Linear contrasts were computed to estimate effects of interest (e.g., faces vs other categories). Fixed-effect analyses were conducted to estimate the average effects across runs within each participant.

Manual definition of FG face-selective regions in individual participants. Face-selective regions on the lateral FG were manually delineated for each hemisphere based on individual, thresholded face-selective activation maps created for each participant ($Z > 1.65$; $p < 0.05$; uncorrected; Fig. 1*A*). Between the two datasets, everything was different—from the number of participants to the scan parameters, the stimuli, and the statistical contrasts used to identify face-selective regions. Thus, the fact that the relationship between gyral crowns and face selectivity generalizes to completely different datasets supports the strength of this structural–functional relationship. Importantly, we did not change any parameters when defining face-selective regions from the prior studies (Jiahui et al., 2018; Chen et al., 2023). We used identical ROIs to conduct the novel analyses in the present study (which were shown to be face selective; iahui et al., 2023, their Fig. S3). Furthermore, using a different contrast for each dataset ensures that our findings are not limited to the contrast used or the stimuli in the experiment. Indeed, previous research has already closely examined how the statistical contrast, voxel size, and amount of data affects the definition, size, and anatomical location of pFus-faces/FFA-1 and mFus-Faces/FFA-2 (Pinsk et al., 2009; Weiner and Grill-Spector, 2010, 2013; McGugin et al., 2012; Weiner et al., 2017a). The present approach was guided by these previous findings. From these thresholded maps, ROIs were labeled as either mFus-faces/FFA-2 or pFus-faces/FFA-1 based on previously published criteria differentiating the cortical location of the two regions relative to sulci within and surrounding the FG (Fig. 1*A*; Weiner et al., 2014; Weiner, 2019; Chen et al., 2023). Specifically, mFus-faces/FFA-2 is located adjacent to the anterior tip of the mid-fusiform sulcus (MFS), whereas pFus-faces/FFA-1 is located on the posterior aspect of the FG, extending into the occipitotemporal sulcus (OTS; Fig. 1*A*; Weiner et al., 2014; Weiner, 2019; Chen et al., 2023). To define each region in the DP and NT sample, K.S.W. identified each region manually on the individual thresholded face-selective map and then authors E.H.W. and J.P.K. labeled these regions in FreeSurfer using *tksurfer* tools (https://surfer.nmr.mgh.harvard.edu/fswiki/TkSurfer). As in prior work (Chen et al., 2023), we used a liberal threshold for the main reason that we did not want to artificially inflate the "separate" group (described below) by using a strict threshold or the "continuous" group (described below) by using a too liberal threshold. Crucially, these regions were defined blind to the identity of all participants (i.e., whether or not they were an NT or DP). The inflated cortical surfaces presented in Figure 1 were generated with Freeview (https://surfer.nmr.mgh.harvard.edu/fswiki/FreeviewGuide). The FG face-selective regions were defined in the HCP sample in our prior work by X.C., Z.Z., and K.S.W. (Chen et al., 2023).

Quantifying the incidence rates and pattern of FG face-selective regions. We categorized the spatial organization of mFus-faces/FFA-2 and pFus-faces/FFA-1 into three types or topological groups as in prior work in over 1,000 participants (Chen et al., 2023): separate, continuous, and single. The "separate" group consisted of two cortically distinct face-selective regions in a given hemisphere that were separated by a cortical gap (Fig. 1*B*). The "continuous" group consisted of two regions that were identifiable and contiguous but could be separated based on previously proposed anatomical criteria using cortical folding (Fig. 1*B*; Weiner et al., 2014; Weiner, 2019; Chen et al., 2023). Note that the most likely factor contributing to the two regions being continuous is the spatial coarseness of the BOLD signal. That is, there is likely a cortical gap in these individuals, but the coarseness of the spatial spread of the BOLD signal causes the two regions to blur together (Chen et al., 2023). The "single" group consisted of one region in which either mFus-faces/FFA-2 or pFus-faces/FFA-1, but not both, was identifiable in a given hemisphere (Fig. 1*B*). After determining these three groups, we summarized the incidence rate of each group (DP, NT) by quantifying how many hemispheres had (1) two or <2 face-selective regions and (2) each topological type.

Defining the parahippocampal place area (PPA) in individual participants. To assess whether group-related results were specific to the FG face-selective regions, we leveraged a cross-validated probabilistic map of the PPA, which resides within the collateral sulcus (CoS) across individuals (Weiner et al., 2018), and projected it to each individual's native space using the mri_surf2surf function in FreeSurfer (Fischl and Dale, 2000).

Defining the FG in individual participants. Given prior research identifying that the FG was smaller in DP (Behrmann et al., 2007) and in other developmental disorders with alterations in face recognition (i.e., ASD and Williams syndrome; van Kooten et al., 2008; Golarai et al., 2010), we sought to replicate these findings. To do so, we leveraged the association region for the lateral FG in the Destrieux parcellation (G_oc-temp_lat-fusifor), which is automatically identified in each FreeSurfer cortical reconstruction (Destrieux et al., 2010).

Quantifying surface area, thickness, and gyral crown height. As in prior work (Chen et al., 2023), the surface area (in squared millimeters) and average cortical thickness (in millimeters) of each region were extracted with the mris_anatomical_stats function in FreeSurfer (Fischl and Dale, 2000). Given that we leveraged a probabilistic map of the PPA in the present study, we did not examine the surface area of this region; however, cortical thickness and gyral height were still examined. The maximum gyral height ("gyral crown"; quantified as the minimum value of the FreeSurfer .sulc file for each FG face-selective region; Dale et al., 1999; Fischl et al., 1999a,b) of each region was extracted using custom Python code leveraging various functions from the numpy, pandas,

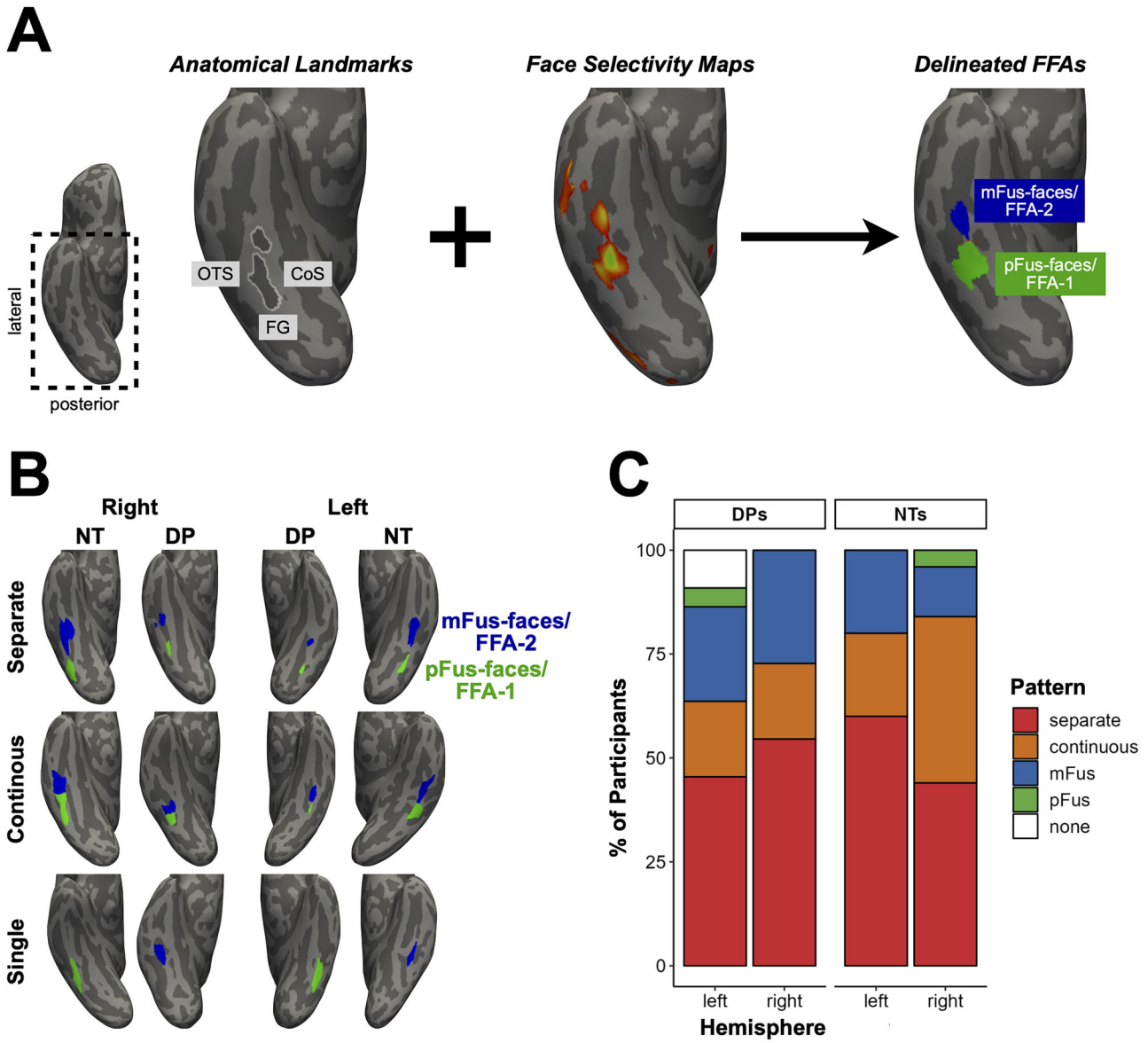

Figure 1. Topographical patterning of pFus-faces/FFA-1 and mFus-faces/FFA-2 does not differ between DPs and NTs. ***A***, Methodology to identify pFus-faces/FFA-1 and/or mFus-faces/FFA-2 in individual participants. Inflated cortical surface reconstruction of a right hemisphere (inset for the location of zoomed portion) from an example NT participant displaying the process for identifying face-selective regions on the lateral FG at the individual level. Face-selective regions were manually defined on the lateral FG in 22 DPs and 25 NTs by using individual anatomical landmarks [OTS, occipitotemporal sulcus; CoS, collateral sulcus; MFS, mid-fusiform sulcus (white outline)] and face-selective maps (middle hemisphere; faces vs objects, $Z > 1.65$; $p < 0.05$, uncorrected). These FG face-selective regions were labeled as either mFus-faces/FFA-2 or pFus-faces/FFA-1 in each hemisphere based on previously published criteria (Weiner et al., 2014). ***B***, FG face-selective regions are displayed for 12 randomly selected hemispheres (one example of each pattern in each hemisphere for each group). Hemispheres are zoomed in on the VTC as in ***A***. Top row, separate group; middle row, continuous group; bottom row, single group. Left two columns, right hemispheres; right two columns, left hemispheres. For each pattern and hemisphere, the outer hemisphere is from an NT, whereas the inner hemisphere is from a DP. ***C***, Bar plot visualizing the incidence of the topographical patterns (colors; see key) as a function of hemisphere (*x*-axis) and group (left: DPs; right: NTs). The incidence (0, 1, or 2 regions) and pattern (see key) of the face-selective regions did not significantly differ between groups (all $p > 0.05$).

nilearn, and nibabel packages (from Miller et al., 2021). Note that values in the .sulc file are calculated based on how far removed a vertex is from what is referred to as a "mid-surface," which is determined computationally so that the mean of the displacements around this "mid-surface" is zero. Thus, generally, gyri have negative values, while sulci have positive values. Therefore, the corresponding maximum gyral height of each region was quantified based on this assignment. These neuroanatomical features are shown visually in Figure 2.

Quantification and statistical analysis

Fisher's exact tests were carried out to compare the incidence rates of face-selective regions and the three topographical types between groups with the fisher.test function from the stats package. Two-way mixed–model ANOVAs were implemented for each quantitative metric (surface area, gyral crown height, average cortical thickness) with the lme and anova functions from nlme and stats packages for each region (mFus-faces/FFA-2, pFus-faces/FFA-1) separately. Hemisphere (left, right) was a within-participant factor, and group (DP, NT) was a between-participant factor. Effect sizes for the significant effects are reported with the partial eta-squared (η^2) metric, computed with the eta_squared function from the effectsize package. Next, we correlated the properties of mFus-faces/FFA-2 and pFus-faces/FFA-1 to face perception ability (as measured by performance on the CFMT; Duchaine and Nakayama, 2006). Spearman rank-order correlations (r_s) and p value calculations were implemented with the cor.test function from the stats package. We used r_s to be less influenced by any potential outliers. For

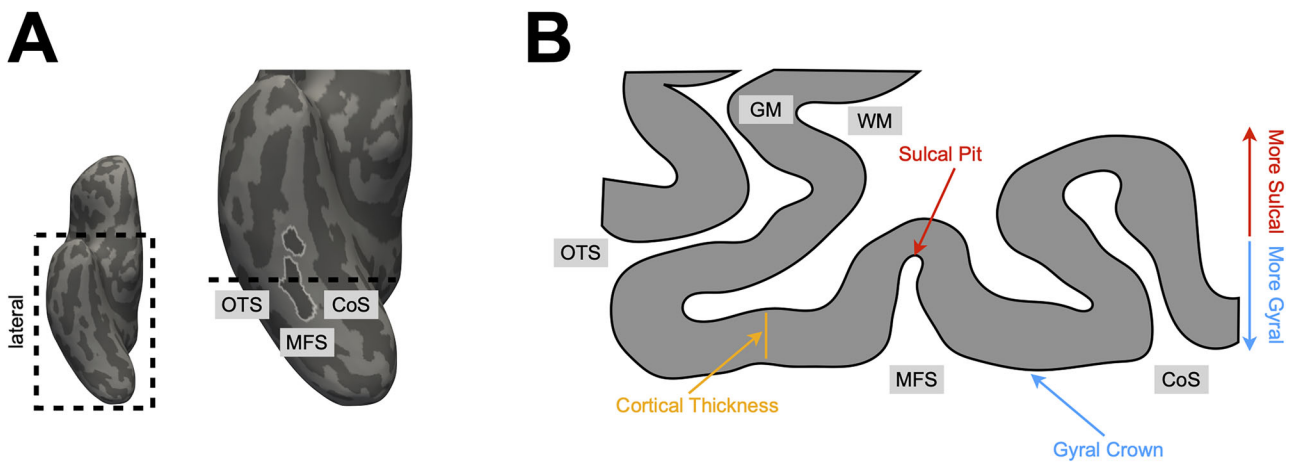

Figure 2. Visualization of sulcal features in VTC. ***A***, Inflated cortical surface (the same from Fig. 1; sulci, dark gray; gyri, light gray) depicting the three key sulci in VTC. The MFS (outlined in white) is a longitudinal sulcus dividing the FG into lateral and medial partitions, flanked by the OTS laterally and the CoS medially (inset for location of zoomed portion; Weiner et al., 2014). ***B***, Artistic rendition of a coronal slice hypothetically taken from the dotted line in A (WM, white matter; GM, gray matter). This coronal slice depicts the distinctive ω pattern of the MFS, OTS, and CoS, where the MFS is the shallower sulcus flanked by the deeper CoS and OTS (Weiner et al., 2014). Also included are labels to depict the morphological features of sulci used in the present study (see Materials and Methods). Specifically, in FreeSurfer, gyral height and sulcal depth values are determined based on how far a given vertex is from a hypothetical "mid-surface" (zero) point between sulci and gyri. Gyri are quantified as more negative values (blue arrow), and sulci are quantified as more positive values (red arrow). The gyral crown and sulcal pit are the highest and lowest points for a given sulcus and gyrus, respectively. Cortical thickness is the thickness of the gray matter layer of the cortex (orange arrow and line).

each correlation, we first tested for a relationship across hemispheres, followed up by testing within each hemisphere separately. To quantify whether there was an indirect effect of gyral crown height on the relationship between mFus-faces/FFA-2 properties and CFMT scores, we implemented a bootstrapped (with 1,000 simulations) causal mediation analysis with the mediate function from the mediation package. Results for the mediation analyses are reported with the bootstrapped average causal mediation effect alongside the 95% confidence interval. Plots were created with the ggplot2 package. These analyses were also performed for features of the lateral FG (surface area) and PPA (gyral crown height and cortical thickness).

All statistical tests and data visualization were implemented in R (v4.0.1; https://www.r-project.org/) via RStudio (RStudio v.2021.09.0 + 351; https://posit.co/). We ensured that all statistical analyses held when removing the DP who did not reach −2 SDs on two of three diagnostic tests. All results held (see Text S1 for full results). Participant age, sex, and handedness, as well as the cortical surface area, were included as control variables. $p < 0.05$ was considered significant for any main effect or interaction after controlling for multiple comparisons (via the false discovery rate).

Data and code availability

Processed data used for the present project have been deposited on GitHub and are publicly available as of the date of publication (https://github.com/cnl-berkeley/stable_projects/tree/main/GyralCrowns_FaceProcessing). All original code used for the present project has also been deposited on Github and is publicly available as of the date of publication. Any additional information required to reanalyze the data reported in this paper is available from the lead contact, Kevin Weiner (kweiner@berkeley.edu), upon request.

Results

Incidence rates of FG face-selective regions do not differ between DPs and NTs

Manually delineating FG face-selective regions in 22 DPs (44 hemispheres) and 25 NTs (50 hemispheres; see Materials and Methods and Fig. 1*A*,*B*) revealed that at least one face-selective region was identifiable in every hemisphere in NTs and in all but two DP hemispheres (Fig. 1*C*). In NTs, 82% (left, 80%; right, 84%) and in DPs, 68.18% (left, 63.64%; right, 72.73%; Fig. 1*C*) had two face-selective regions on the FG. As in prior work (Chen et al., 2023), these incidence rates could be further categorized into one of three different types in a given hemisphere: separate, continuous, or single (see Materials and Methods; Fig. 1*B*). The most common was the separate group, in which 52% of NT hemispheres (LH, 60%; RH, 44%) and 50% of DP hemispheres (LH, 45.46%; RH, 54.55%) contained two face-selective regions that were separated by a cortical gap of several millimeters (Fig. 1*B*,*C*). In the continuous group, which consisted of 30% of cases in NTs (LH, 20%; RH, 40%) and 18.18% of cases in DPs (LH, 18.18%; RH, 18.18%), mFus-faces/FFA-2 and pFus-faces/FFA-1 were identifiable and largely contiguous (Fig. 1*B*,*C*). Specifically, the former was identified as the functional region located adjacent to the anterior tip of the MFS, while the latter was identified as the functional region located adjacent to the posterior extent of the MFS extending into the lateral FG and the nearby OTS (Fig. 1; Weiner et al., 2014; Weiner, 2019; Chen et al., 2023). In 18% of NT cases (LH, 20%; RH, 16%) and 27.27% of DP cases (LH, 27.27%; RH, 27.27%), either mFus-faces/FFA-2 or pFus-faces/FFA-1, but not both, was identifiable in a given hemisphere based on the criteria just described (Fig. 1*B*,*C*). A single mFus-faces-FFA/2 was more common than a single pFus-faces/FFA-1 in both NTs (*mFus*, LH, 20%; RH, 12%; *pFus*, LH, 0%; RH, 4%; $X^2 = 5.44$; $p = 0.01$) and DPs (*mFus*, LH, 22.73%; RH, 27.27%; *pFus*, LH, 4.55%; RH, 0%; $X^2 = 8.33$; $p = 0.003$). In the left hemisphere, two DPs (9.09%) did not have an identifiable mFus-faces/FFA-2 or pFus-faces/FFA-2 (Fig. 1*C*). These results are similar to a recent study from our laboratory (Chen et al., 2023), which found that the highest percentage of participants was in the separate group, then the continuous group, and then the single group. The percentages of mFus-faces/FFA-2 and pFus-faces/FFA-1 combinations did not differ between DPs and NTs (both, $p = 0.20$; left, $p = 0.49$; right, $p = 0.26$; Fig. 1*C*).

The gyral crown and surface area of FG face-selective regions differ between DPs and NTs

As recent findings show a relationship between cortical folding in relation to category-selective regions in the high-level visual cortex (Weiner et al., 2014; Abbasi et al., 2020; Arcaro et al., 2020;

Natu et al., 2021), we tested if the gyral crown (highest point of cortical folding) of each FG face-selective region differed between groups. We also considered cortical thickness as it is a common measure examined in FG face-selective regions (Bi et al., 2014; McGugin et al., 2016, 2020; Zebrowitz et al., 2016; Chen et al., 2023). Crucially, these features were selected based on the functional boundaries of each region and, thus, are not necessarily dependent on any given cortical landmark (e.g., a specific sulcus or gyrus). Mixed-model ANOVAs for each region (mFus-faces/FFA-2, pFus-faces/FFA-1) with the hemisphere (left, right) and group (NT, DP) as factors revealed a main effect of group on gyral crown height for each region (mFus-faces/FFA-2, $F_{(1,42)} = 11.07$; $p = 0.007$; $\eta^2 = 0.21$; pFus-faces/FFA-1, $F_{(1,39)} = 12.01$; $p = 0.005$; $\eta^2 = 0.24$), such that the gyral crown height of both FG face-selective regions was lower in DPs (mFus-faces/FFA-2, mean ± SE = −3.49 ± 0.36; pFus-faces/FFA-1, mean ± SE = −4.07 ± 0.41) compared with NTs (mFus-faces/FFA-2, mean ± SE = −5.02 ± 0.27; pFus-faces/FFA-1, mean ± SE = −6.38 ± 0.36; Fig. 3*A*). There were no main effects of hemisphere or hemisphere and group interactions on gyral crown height for either region ($ps > 0.28$; Fig. 3*A*). In contrast to the main effect of gyral crown height, there was no main effect of group on cortical thickness for either region ($ps > 0.46$; Fig. S1*A*). Participant sex, age, and handedness did not relate to the gyral crown height of either region ($ps > 0.10$). There were also no main effects of hemisphere or hemisphere and group interactions on cortical thickness for either region ($ps > 0.65$; Fig. S1*A*), and participant sex, age, and handedness did not relate to the cortical thickness of either region ($ps > 0.50$).

We also wanted to examine whether the morphological properties (i.e., surface area) of the FG face-selective regions differed between groups. To do so, we next implemented mixed-model ANOVAs for each region with factors of the hemisphere (left, right) and group (NT, DP) to test whether the size (surface area in square millimeters) of each FG face-selective region differed between groups. The two DP hemispheres without an FG face-selective region were not included in the analyses. These analyses revealed two main findings. First, there was a main effect of group on the size of mFus-faces/FFA-2 ($F_{(1,42)} = 8.21$; $p = 0.025$; $\eta^2 = 0.16$), such that the surface area was generally smaller in DPs (mean ± SE = 133 ± 15.9 mm^2) compared with NTs (mean ± SE = 209 ± 19.5 mm^2; Fig. 3*B*, left). Second, there was no main effect of group on the size of pFus-faces/FFA-1 ($F_{(1,39)} = 0.53$; $p = 0.46$; $\eta^2 = 0.01$; DP, mean ± SE = 152 ± 19.2 mm^2; NT, mean ± SE = 171 ± 14.2 mm^2; Fig. 3*B*, right). This difference in the size is consistent with a previous preprint in a smaller group of DPs ($N = 7$) showing that the volume of mFus-faces/FFA-2, but not pFus-faces/FFA-1, was smaller in DPs compared with NTs (Witthoft et al., 2016). There was also no main effect of hemisphere or a hemisphere and group interaction on the size of either region ($ps > 0.37$; Fig. 3*B*). Participant sex, age, and handedness did not relate to the size of either region ($ps > 0.33$).

Gyral crown height correlates with the surface area of FG face-selective regions

Next, we tested if the neuroanatomical and morphological features of FG face-selective measures were correlated with the surface area of FG face-selective regions. Gyral crown height was related to the size of both regions across hemispheres, such that the higher the gyral crown within the anatomical locus within the FG, the larger the surface area of the face-selective region (mFus-faces/FFA-2, $r_s = -0.44$; $p = 0.00001$; pFus-faces/FFA-1, $r_s = -0.30$, $p = 0.01$; Fig. 4*A*). In both regions, this relationship was stronger in the right hemisphere (mFus-faces/FFA-2, $r_s = -0.59$; $p = 0.0001$; pFus-faces/FFA-1, $r_s = -0.36$; $p = 0.025$) compared with the left (mFus-faces/FFA-2, $r_s = -0.29$; $p = 0.053$; pFus-faces/FFA-1, $r_s = -0.26$; $p = 0.13$; Fig. 4*A*). Conversely, cortical thickness was unrelated to the size of either region ($ps > 0.47$; Fig. S1*B*).

To test whether this novel relationship between gyral crowns and the surface area of FG face-selective regions was also present in a larger sample that used a different methodology (e.g., task details, statistical threshold, etc.), we leveraged the prior definitions of FG face-selective regions from 1,053 participants

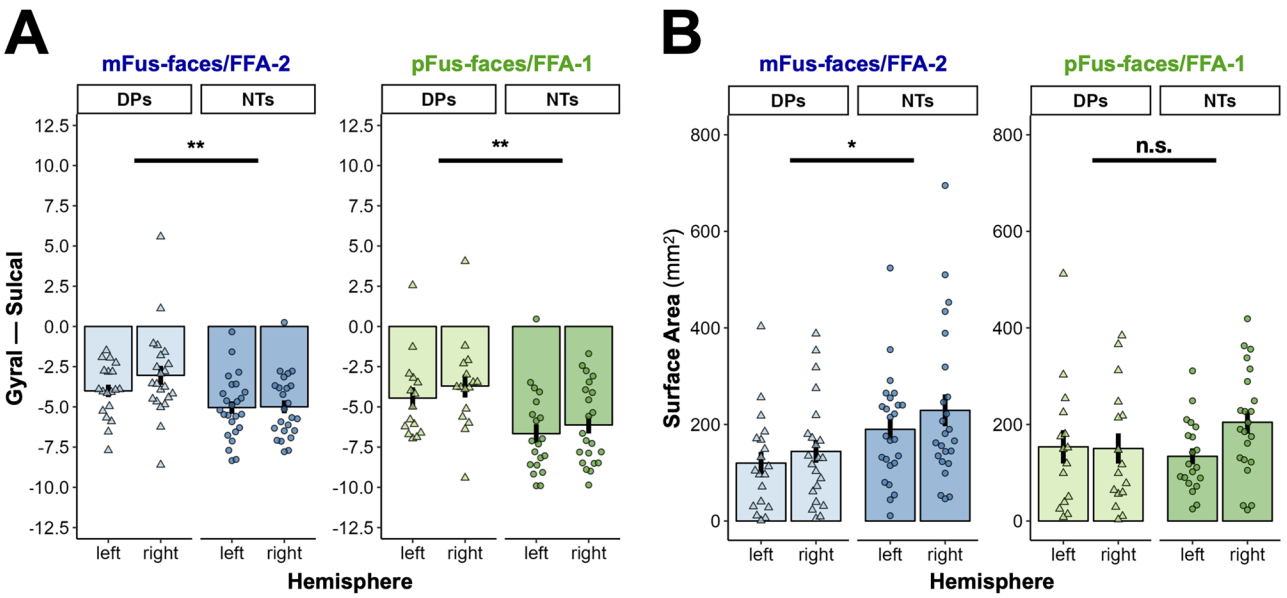

Figure 3. Gyral crown height and surface area of FG face-selective regions differ between DPs and NTs. ***A***, Bar plots and error bars (mean ± SE) visualizing region maximal gyral height ("gyral crown"; in FreeSurfer units, the more negative value indicates higher gyral height) as a function of hemisphere (*x*-axis) and group (left, DPs; right, NTs) for both mFus-faces/FFA-2 (left plot) and pFus-faces/FFA-1 (right plot). Individual dots represent individual values for each participant (DPs, triangles; NTs, circles). The horizontal line and asterisks visualize the statistical significance of the group difference for gyral crowns across groups. ***B***, Same as ***A*** but for the region surface area (in square millimeter; $^{**}p < 0.01$; n.s., $p > 0.05$).

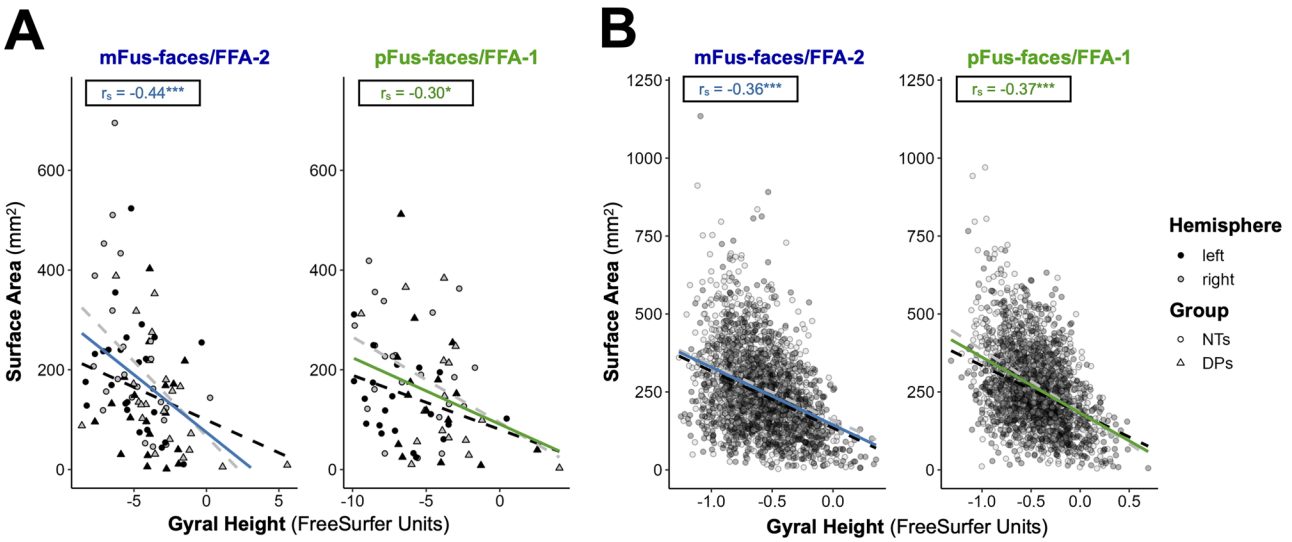

Figure 4. Gyral crown height is related to the surface area of FG face-selective regions. ***A***, Scatterplot of maximal gyral height ("gyral crown"; in FreeSurfer units, the more negative value indicates higher gyral height; *x*-axis) and surface area (in square millimeter; *y*-axis) for mFus-faces/FFA-2 (left) and pFus-faces/FFA-1 (right). The solid, colored line corresponds to the best-fit line across hemispheres alongside the corresponding correlation coefficient (r_s) and *p* values (asterisks). The best-fit lines for the left and right hemispheres are also shown as dashed lines colored according to the key. Individual dots represent individual values for each participant which are colored by hemisphere (left, black; right, white; see key) and shaped according to the group of that individual (DPs, triangles; NTs, circles; see key). ***B***, Same format as ***A***, but for the HCP sample ($N = 1{,}053$; Chen et al., 2023; ***$p < 0.001$; **$p < 0.01$; *$p < 0.05$).

(478 males, mean age = 29 years old; 2,106 hemispheres) from the HCP (for additional sample and methodological details, see Chen et al. (2023). This analysis showed that the relationship between gyral crown height and the size of FG face-selective regions was replicated for both mFus-faces/FFA-2 (across hemispheres, $r_s = -0.36$; $p < 2.2 \times 10^{-16}$; left hemisphere, $r_s = -0.38$; $p < 2.2 \times 10^{-16}$; right hemisphere, $r_s = -0.33$; $p < 2.2 \times 10^{-16}$; Fig. 4*B*, left) and pFus-faces/FFA-1 (across hemispheres, $r_s = -0.37$; $p < 2.2 \times 10^{-16}$; left hemisphere, $r_s = -0.36$; $p < 2.2 \times 10^{-16}$; right hemisphere, $r_s = -0.39$; $p < 2.2 \times 10^{-16}$; Fig. 4*B*, right). The relationship between cortical thickness and size was weak for both regions in the HCP sample (Fig. S1*C*).

The size of mFus-faces/FFA-2, but not pFus-faces/FFA-1, correlates with face processing ability and is mediated by gyral crown height

To build upon prior work showing a relationship between face processing ability and the size of the FFA (Golarai et al., 2007, 2010; Furl et al., 2011; Elbich and Scherf, 2017), but which did not consider individual FG face-selective regions, we tested whether the size of each FG face-selective region was also correlated with performance on the CFMT (Duchaine and Nakayama, 2006). In addition, if a correlation was significant, we assessed if this relationship was mediated by gyral crown height. Importantly, our voxel selection criteria for ROI definitions were defined a priori and were completely independent of the behavioral measures. Concomitantly, the relationship between the surface area of face-selective regions and CFMT performance is orthogonal to the voxel selection process (Nichols and Poline, 2009; Poldrack and Mumford, 2009; Vul et al., 2009).

For mFus-faces/FFA-2, there was a positive relationship between CFMT performance and the ROI size, such that the larger the surface area, the better face processing performance (across hemispheres, $r_s = 0.33$; $p = 0.001$; left hemisphere, $r_s = 0.38$; $p = 0.011$; right hemisphere, $r_s = 0.31$; $p = 0.041$; Fig. 5*A*, left). In contrast, there was not a significant relationship between CFMT performance and the size of pFus-faces/FFA-1 (across hemispheres, $r_s = 0.13$; $p = 0.25$; left hemisphere, $r_s = 0.008$; $p = 0.96$; right hemisphere, $r_s = 0.25$; $p = 0.13$; Fig. 5*A*, right). The size correlations were modestly different between regions (across hemispheres, Fisher's $Z = 1.31$; $p = 0.095$; left hemisphere, Fisher's $Z = 1.66$; $p = 0.049$; right hemisphere, Fisher's $Z = 0.28$; $p = 0.38$). Interestingly, these findings are similar to a previously published preprint in a much smaller sample size of DPs ($N = 7$) in which there was a marginally significant relationship between the volume of mFus-faces/FFA-2 and CFMT ($r = 0.49$; $p = 0.08$), but not between the volume of pFus-faces/FFA-1 and CFMT ($r = 0.28$; $p = 0.32$; Witthoft et al., 2016).

Examining the relationship between the gyral crown height of mFus-faces/FFA-2 and CFMT performance also revealed a significant overall relationship (across hemispheres, $r_s = -0.32$; $p = 0.002$) with stronger effects in the right hemisphere ($r_s = -0.39$; $p = 0.007$) than in the left hemisphere ($r_s = -0.24$; $p = 0.11$; Fig. 5*B*, left). A similar relationship between the gyral crown height of pFus-faces/FFA-1 and CFMT performance was observed (across hemispheres, $r_s = -0.39$; $p = 0.007$; left hemisphere, $r_s = -0.40$; $p = 0.018$; right hemisphere, $r_s = -0.42$; $p = 0.009$; Fig. 5*B*, right). As an additional observation, DP participants with particularly low gyral height values (as seen in Fig. 3*A*) that were subsequently identified as outliers—based on the interquartile range method—tended to exhibit lower CFMT performance, particularly in pFus-faces/FFA-1 (Fig. S2). There was no relationship between cortical thickness of either region and CFMT ($ps > 0.32$; Fig. S1*D*).

Finally, given the relationship between gyral crown height and the size of mFus-faces/FFA-2 (Fig. 4), we sought to determine whether gyral crown height mediated the observed relationship between the size of mFus-faces/FFA-2 and CFMT performance with causal mediation analyses. Computing this indirect effect of gyral crown height from 1,000 bootstrapped simulations with the bias-corrected method revealed that gyral crown height mediated the relationship between the size of mFus-faces/FFA-2 and CFMT (indirect effect [95% CI] = 0.008 [0.0005, 0.02]; $p = 0.04$).

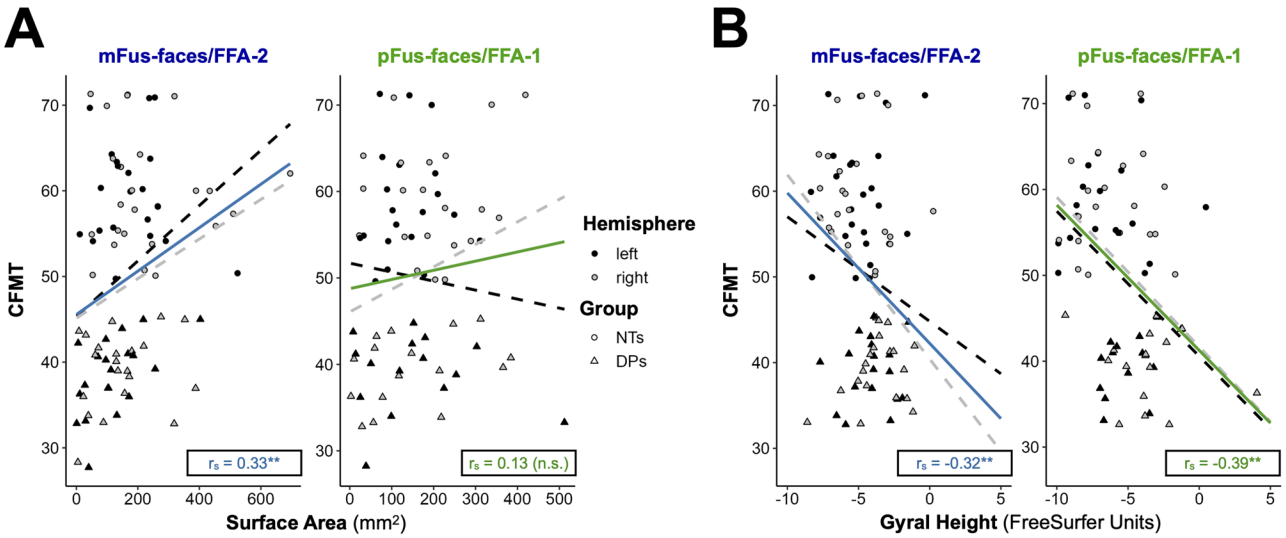

Figure 5. Size and gyral crown height of FG face-selective regions selectively correlate with face recognition ability. ***A***, Scatterplot of surface area (in square millimeter; *x*-axis) and CFMT (*y*-axis) performance for mFus-faces/FFA-2 (left) and pFus-faces/FFA-1 (right). The solid, colored line corresponds to the best-fit line across hemispheres alongside the corresponding correlation coefficient (r_s) and *p* values. The best-fit lines for the left and right hemispheres are also shown as dashed lines colored according to the key. Individual dots represent individual values for each participant which are colored by hemisphere (left, black; right, white; see key) and shaped according to the group of that individual (DPs, triangles; NTs, circles; see key). ***B***, Same as ***A***, but for maximal gyral crown height (in FreeSurfer units: the more negative value indicates higher gyral crown height; $^{**}p < 0.01$; n.s., $p > 0.05$).

Neuroanatomical features of the PPA do not differ between DPs and NTs or relate to face processing ability

As a control analysis, we also examined whether the neuroanatomical features of a nonface-selective region differed between DPs and NTs by leveraging a probabilistic map of the PPA (see Materials and Methods; Fig. S3*A*; Weiner et al., 2018). Mixed-model ANOVAs with the hemisphere (left, right) and group (NT, DP) as factors found no main effect of group on PPA gyral crown height ($F_{(1,42)} = 3.68$; $p = 0.12$; $\eta^2 = 0.08$; Fig. S3*B*) or PPA cortical thickness ($F_{(1,42)} = 3.39$; $p = 0.25$; $\eta^2 = 0.07$; Fig. S3*C*). There were no other effects for the control variables of hemisphere, participant sex, age, and handedness ($ps > 0.12$). Features of the PPA did not correlate with CFMT performance ($ps > 0.07$; Fig. S3*D*,*E*).

The size of the lateral FG differs between DPs and NTs, but does not relate to face processing ability

Prior studies in DP (Behrmann et al., 2007) and other developmental disorders with impaired face recognition abilities (i.e., Williams and autism spectrum disorders; van Kooten et al., 2008; Golarai et al., 2010) have found that the FG is smaller in individuals with these disorders. Therefore, we sought to test the replicability and generalizability of this relationship in the present sample using the G_oc-temp_lat-fusifor region from the Destrieux parcellation (see Materials and Methods; Fig. S4*A*; Destrieux et al., 2010). Mixed-model ANOVAs, controlling for the overall brain size, with factors of hemisphere (left, right) and group (NT, DP) on the lateral FG size (surface area in square millimeter) found a main effect of group ($F_{(1,42)} = 7.87$; $p = 0.012$; $\eta^2 = 0.16$), such that the surface area was generally smaller in DPs (mean ± SE = 1,230 ± 44.2 mm^2) compared with NTs (mean ± SE = 1,335 ± 31.9 mm^2; Fig. S4*B*). There were also main effects of hemisphere ($F_{(1,44)} = 7.25$; $p = 0.013$; $\eta^2 = 0.14$; left, mean ± SE = 1,235 ± 32.5 mm^2; right, mean ± SE = 1,336 ± 42.6 mm^2; Fig. S4*B*), handedness ($F_{(1,42)} = 12.23$; $p = 0.002$; $\eta^2 = 0.23$; left, mean ± SE = 1,143 ± 69.7 mm^2; right, mean ± SE = 1,315 ± 28.5 mm^2), and sex ($F_{(1,42)} = 50.92$; $p = 0.00000003$; $\eta^2 = 0.55$; males, mean ± SE = 1,175 ± 24.6 mm^2; females, mean ± SE = 1,481 ± 44.9 mm^2). There was no main effect of age or interactions ($ps > 0.15$). The size of the lateral FG did not correlate with CFMT performance ($ps > 0.05$; Fig. S4*C*).

Discussion

In the present study, we examined the structure and function of separate FG face-selective regions (mFus-faces/FFA-2 and pFus-faces/FFA-1) in DPs relative to NTs. We showed that the incidence and topographical location of these regions relative to cortical folding was organized similarly between DPs and NTs. The lack of differences regarding the topographical arrangement of the FG face-selective regions is consistent with previous findings showing that DPs generally have a comparable gross functional organization of VTC to NTs (Avidan et al., 2005, 2014; Avidan and Behrmann, 2009; Garrido et al., 2009; Zhang et al., 2015; Jiahui et al., 2018), which we now extend to a finer scale (i.e., considering multiple FG face-selective regions and tertiary sulci in VTC).

Despite these observed topographical similarities, the more anteriorly located mFus-faces/FFA-2 was smaller in DPs compared with NTs, while this was not the case for the more posterior pFus-faces/FFA-1. We further showed that the surface area of mFus-faces/FFA-2, but not pFus-faces/FFA-1, was related to CFMT performance. Our results indicate a new relationship between gyral crowns and the surface area of FG face-selective regions: gyral crown height, but not cortical thickness, was related to the surface area of FG face-selective regions and differed between DPs and NTs. This structural–functional effect generalized to a sample of 1,053 participants from the HCP, indicating a new structural–functional relationship of two anatomically and functionally distinct face-selective regions on the FG (Weiner et al., 2010; Chen et al., 2023). We also replicated and generalized prior findings in DP (Behrmann et al., 2007) and other developmental disorders with impaired face recognition abilities (i.e., Williams syndrome and ASD; van Kooten et al., 2008; Golarai et al., 2010) by showing that the FG surface area is smaller in DPs. Below, we discuss these results in the context of (1) coupling between local anatomical features and

category selectivity in VTC and (2) functional and structural differences between NTs and DPs.

Coupling between local anatomical features and category selectivity in VTC

The present findings build on recent studies identifying a relationship between local anatomical features and category selectivity in VTC. In medial VTC, Natu and colleagues identified a relationship between deep sulcal points in the CoS and place selectivity in children and young adults (Natu et al., 2021). In lateral VTC, Cachia and colleagues identified a relationship between a functional region selective for visual words and a gyral gap in the OTS (Cachia et al., 2018). Building on that work, Bouhali and colleagues showed that longitudinal changes in the OTS gyral gap correlated with longitudinal changes in reading ability—changes that were mediated by underlying white matter properties (Bouhali et al., 2024). Furthermore, previous work also showed a coupling between the anterolateral tip of the MFS and mFus-faces/FFA-2 (Weiner, 2019) and that the MFS was shorter in DPs and its length correlated with face recognition ability (Parker et al., 2023). Here, we show that the highest local gyral point within mFus-faces/FFA-2 contributes to this structural–functional coupling between cortical folding and face selectivity.

This coupling between local anatomical features and category selectivity also extends to nonhuman primates. For example, there is also a relationship between "bumps" in the superior temporal sulcus and face selectivity in NHPs (Arcaro et al., 2020). Thus, there is growing evidence that local anatomical features are better anatomical predictors of category selectivity in high-level visual cortex across species than gross macroanatomical landmarks (e.g., entire sulci or gyri). As a final point in this section, the present findings contribute to work suggesting the importance of gyral crown height and its contributions to brain structure and function (Zhang et al., 2022, 2023), as well as a potential functional relevance of a latitude/longitude coordinate system of sulcal pits and gyral crowns and their relevance to face and place selectivity in human VTC (Auzias et al., 2013), which can also be explored in future work.

Functional and structural differences between NTs and DPs: connectivity, cortical folding, and microarchitecture

There is a known relationship between white matter architecture and cortical folding. For example, long-range white matter fibers have a "gyral bias" (also referred to as "gyral blades"; Van Essen et al., 2014; Cottaar et al., 2021). An intriguing possibility is that the relationship among gyral crown height, functional features of mFus-faces/FFA-2, and face processing ability identified in the present study indicates that this anatomical location could be an integration zone across cortical networks. Recent electrical brain stimulation (EBS) studies support this possibility: EBS delivered to the more posterior pFus-faces/FFA-1 shows effects that are specific to perceptual aspects of faces, while EBS delivered to the more anterior mFus-faces/FFA-2 shows effects supporting an integration between networks that are related to semantics such as naming and person knowledge (Parvizi et al., 2012; Rangarajan et al., 2014; Schrouff et al., 2020).

While the present data cannot establish causality, an important open question is whether reduced gyral height is a cause or a consequence of altered face processing. One possibility is that genetic factors, cellular mechanisms, and/or biomechanical forces influencing cortical folding and sulcal/gyral morphology (e.g., differential patterns of sulcal pits and gyral crowns; Im and Grant, 2019; Huang et al., 2023) may shape local white matter architecture, which in turn constrains the functional specialization of fusiform regions and then ultimately impacts face processing ability (Hilgetag and Barbas, 2005, 2006; Borrell, 2018; Kroenke and Bayly, 2018). Alternatively, in light of accumulating evidence that face selectivity develops during late childhood and adolescence, and this development may involve cortical recycling of other representations, prolonged differences in face experience or processing demands, as may occur in DP, could drive plastic changes in cortical architecture (Nordt et al., 2021). Thus, the observed associations may reflect a complex cascade of bidirectional influences across genetic, structural, and experiential levels. Research linking white matter connectivity to gyral crown and sulcal pit morphology (e.g., Van Essen et al., 2014; Mortazavi et al., 2017; Cottaar et al., 2021) further suggests that structural folding patterns could both shape and be shaped by connectivity, providing multiple mechanistic entry points for how gyral height might relate to face processing outcomes.

In addition, incorporating other anatomical features, such as cortical myelin estimates from T1/T2 mapping (Glasser and Van Essen, 2011), quantitative MR measures (Mezer et al., 2013), or even cytoarchitecture—if and when it is measurable in the living human brain—will be critical for understanding how distinct structural properties jointly contribute to functional specialization across FG functional subregions between DPs and NTs. For instance, previous DP studies have identified structural and functional abnormalities in VTC (Behrmann et al., 2007; Thomas et al., 2009; Zhao et al., 2016, 2018; Tian et al., 2020) and that there could also be cytoarchitectural differences based on recent findings (Kubota et al., 2023, 2025). An integrative hypothesis for future studies would predict that different portions of the same white matter tract could terminate in different functional regions, as previously shown in this journal (Weiner et al., 2016)—and even in the same cytoarchitectonic territory (Weiner et al., 2017b)—in face- and word-selective regions. This hypothesis would suggest that the combination of focal microarchitectonic, cortical folding, and white matter measurements could have predictable power for predicting individual differences in face processing, which can be tested in the future.

Limitations

Future measurements aside, it is important to mention that FG face-selective region surface area and gyral crown height are not necessarily biomarkers for DP. Both measures show substantial overlap between DPs and NTs, indicating that these features are unlikely to serve as categorical diagnostic markers between groups. Instead, they may represent structural dimensions that modulate individual differences in face processing ability and contribute probabilistically to risk for face recognition difficulties, rather than acting as deterministic predictors of DP. It is also worth noting that face processing deficits are evident in ASD (Dawson et al., 2005). Although, we did not collect Autism Spectrum Quotient data for our DP dataset (Jiahui et al., 2018), future studies should investigate the relationship between face processing in ASD and structural features of FG face-selective regions, especially given neuroanatomical alterations in VTC sulci observed in ASD (Ammons et al., 2021; Ramos Benitez et al., 2024).

Conclusion

Altogether, the present findings provide a new anatomical feature to incorporate into theories of how the human brain processes

faces as well as reveal a new neuroanatomical target in clinical populations who have difficulties processing faces. The combination of these findings indicate that there may be smaller group differences in posterior face-selective regions compared with anterior face-selective regions in VTC which leads to a targeted hypothesis for future research: the percentage of DPs with abnormalities in VTC face-selective regions will rise as one moves anatomically forward in the face processing stream. Thus, an immediate goal of future studies is to further understand why the anterior tip of the MFS extending into the lateral mid-FG is a neuroanatomical target between NTs and DPs and if this is a general finding across other populations with difficulties in face processing.

References

Abbasi N, Duncan J, Rajimehr R (2020) Genetic influence is linked to cortical morphology in category-selective areas of visual cortex. Nat Commun 11:709.

Alemán-Gómez Y, et al. (2013) The human cerebral cortex flattens during adolescence. J Neurosci 33:15004–15010.

Ammons CJ, Winslett M-E, Bice J, Patel P, May KE, Kana RK (2021) The mid-fusiform sulcus in autism spectrum disorder: establishing a novel anatomical landmark related to face processing. Autism Res 14:53–64.

Arcaro MJ, Mautz T, Berezovskii VK, Livingstone MS (2020) Anatomical correlates of face patches in macaque inferotemporal cortex. Proc Natl Acad Sci U S A 117:32667–32678.

Auzias G, Lefèvre J, Le Troter A, Fischer C, Perrot M, Régis J, Coulon O (2013) Model-driven harmonic parameterization of the cortical surface: HIP-HOP. IEEE Trans Med Imaging 32:873–887.

Avidan G, Behrmann M (2009) Functional MRI reveals compromised neural integrity of the face processing network in congenital prosopagnosia. Curr Biol 19:1146–1150.

Avidan G, Hasson U, Malach R, Behrmann M (2005) Detailed exploration of face-related processing in congenital prosopagnosia: 2. Functional neuroimaging findings. J Cogn Neurosci 17:1150–1167.

Avidan G, Tanzer M, Hadj-Bouziane F, Liu N, Ungerleider LG, Behrmann M (2014) Selective dissociation between core and extended regions of the face processing network in congenital prosopagnosia. Cereb Cortex 24: 1565–1578.

Barch DM, et al. (2013) Function in the human connectome: task-fMRI and individual differences in behavior. Neuroimage 80:169–189.

Behrmann M, Avidan G, Gao F, Black S (2007) Structural imaging reveals anatomical alterations in inferotemporal cortex in congenital prosopagnosia. Cereb Cortex 17:2354–2363.

Behrmann M, Scherf KS, Avidan G (2016) Neural mechanisms of face perception, their emergence over development, and their breakdown. Wiley Interdiscip Rev Cogn Sci 7:247–263.

Bi T, Chen J, Zhou T, He Y, Fang F (2014) Function and structure of human left fusiform cortex are closely associated with perceptual learning of faces. Curr Biol 24:222–227.

Borrell V (2018) How cells fold the cerebral cortex. J Neurosci 38:776–783.

Bouhali F, Dubois J, Hoeft F, Weiner KS (2024) Unique longitudinal contributions of sulcal interruptions to reading acquisition in children. Elife 13: RP103007.

Cachia A, Roell M, Mangin J-F, Sun ZY, Jobert A, Braga L, Houde O, Dehaene S, Borst G (2018) How interindividual differences in brain anatomy shape reading accuracy. Brain Struct Funct 223:701–712.

Chen X, Liu X, Parker BJ, Zhen Z, Weiner KS (2023) Functionally and structurally distinct fusiform face area(s) in over 1000 participants. Neuroimage 265:119765.

Cottaar M, Bastiani M, Boddu N, Glasser MF, Haber S, van Essen DC, Sotiropoulos SN, Jbabdi S (2021) Modelling white matter in gyral blades as a continuous vector field. Neuroimage 227:117693.

Çukur T, Huth AG, Nishimoto S, Gallant JL (2013) Functional subdomains within human FFA. J Neurosci 33:16748–16766.

Dale AM, Fischl B, Sereno MI (1999) Cortical surface-based analysis. I. Segmentation and surface reconstruction. Neuroimage 9: 179–194.

Davidenko N, Remus DA, Grill-Spector K (2012) Face-likeness and image variability drive responses in human face-selective ventral regions. Hum Brain Mapp 33:2334–2349.

Dawson G, Webb SJ, McPartland J (2005) Understanding the nature of face processing impairment in autism: insights from behavioral and electrophysiological studies. Dev Neuropsychol 27:403–424.

Destrieux C, Fischl B, Dale A, Halgren E (2010) Automatic parcellation of human cortical gyri and sulci using standard anatomical nomenclature. Neuroimage 53:1–15.

Duchaine B, Nakayama K (2005) Dissociations of face and object recognition in developmental prosopagnosia. J Cogn Neurosci 17:249–261.

Duchaine B, Nakayama K (2006) The Cambridge Face Memory Test: results for neurologically intact individuals and an investigation of its validity using inverted face stimuli and prosopagnosic participants. Neuropsychologia 44:576–585.

Duchaine B, Yovel G (2015) A revised neural framework for face processing. Annu Rev Vis Sci 1:393–416.

Duchaine B, Germine L, Nakayama K (2007a) Family resemblance: ten family members with prosopagnosia and within-class object agnosia. Cogn Neuropsychol 24:419–430.

Duchaine B, Yovel G, Nakayama K (2007b) No global processing deficit in the Navon task in 14 developmental prosopagnosics. Soc Cogn Affect Neurosci 2:104–113.

Elbich DB, Scherf S (2017) Beyond the FFA: brain-behavior correspondences in face recognition abilities. Neuroimage 147:409–422.

Engell AD, McCarthy G (2013) Probabilistic atlases for face and biological motion perception: an analysis of their reliability and overlap. Neuroimage 74:140–151.

Finzi D, Gomez J, Nordt M, Rezai AA, Poltoratski S, Grill-Spector K (2021) Differential spatial computations in ventral and lateral face-selective regions are scaffolded by structural connections. Nat Commun 12:2278.

Fischl B, Sereno MI, Dale AM (1999a) Cortical surface-based analysis. II: inflation, flattening, and a surface-based coordinate system. Neuroimage 9:195–207.

Fischl B, Sereno MI, Tootell RB, Dale AM (1999b) High-resolution intersubject averaging and a coordinate system for the cortical surface. Hum Brain Mapp 8:272–284.

Fischl B, Dale AM (2000) Measuring the thickness of the human cerebral cortex from magnetic resonance images. Proc Natl Acad Sci U S A 97:11050–11055.

Furl N, Garrido L, Dolan RJ, Driver J, Duchaine B (2011) Fusiform gyrus face selectivity relates to individual differences in facial recognition ability. J Cogn Neurosci 23:1723–1740.

Garrido L, Furl N, Draganski B, Weiskopf N, Stevens J, Tan GC-Y, Driver J, Dolan RJ, Duchaine B (2009) Voxel-based morphometry reveals reduced grey matter volume in the temporal cortex of developmental prosopagnosics. Brain 132:3443–3455.

Glasser MF, et al. (2013) The minimal preprocessing pipelines for the human connectome project. Neuroimage 80:105–124.

Glasser MF, Van Essen DC (2011) Mapping human cortical areas in vivo based on myelin content as revealed by T1- and T2-weighted MRI. J Neurosci 31:11597–11616.

Golarai G, Ghahremani DG, Whitfield-Gabrieli S, Reiss A, Eberhardt JL, Gabrieli JDE, Grill-Spector K (2007) Differential development of high-level visual cortex correlates with category-specific recognition memory. Nat Neurosci 10:512–522.

Golarai G, Hong S, Haas BW, Galaburda AM, Mills DL, Bellugi U, Grill-Spector K, Reiss AL (2010) The fusiform face area is enlarged in Williams syndrome. J Neurosci 30:6700–6712.

Gomez J, Pestilli F, Witthoft N, Golarai G, Liberman A, Poltoratski S, Yoon J, Grill-Spector K (2015) Functionally defined white matter reveals segregated pathways in human ventral temporal cortex associated with category-specific processing. Neuron 85:216–227.

Gomez J, Barnett MA, Natu V, Mezer A, Palomero-Gallagher N, Weiner KS, Amunts K, Zilles K, Grill-Spector K (2017) Microstructural proliferation in human cortex is coupled with the development of face processing. Science 355:68–71.

Gomez J, Natu V, Jeska B, Barnett M, Grill-Spector K (2018) Development differentially sculpts receptive fields across early and high-level human visual cortex. Nat Commun 9:788.

Hilgetag CC, Barbas H (2005) Developmental mechanics of the primate cerebral cortex. Anat Embryol 210:411–417.

Hilgetag CC, Barbas H (2006) Role of mechanical factors in the morphology of the primate cerebral cortex. PLoS Comput Biol 2:e22.

Huang Y, Zhang T, Zhang S, Zhang W, Yang L, Zhu D, Liu T, Jiang X, Han J, Guo L (2023) Genetic influence on gyral peaks. Neuroimage 280:120344.

Im K, Jo HJ, Mangin J-F, Evans AC, Kim SI, Lee J-M (2010) Spatial distribution of deep sulcal landmarks and hemispherical asymmetry on the cortical surface. Cereb Cortex 20:602–611.
Im K, Grant PE (2019) Sulcal pits and patterns in developing human brains. Neuroimage 185:881–890.
Jiahui G, Yang H, Duchaine B (2018) Developmental prosopagnosics have widespread selectivity reductions across category-selective visual cortex. Proc Natl Acad Sci U S A 115:E6418–E6427.
Jonas J, Rossion B (2021) Intracerebral electrical stimulation to understand the neural basis of human face identity recognition. Eur J Neurosci 54: 4197–4211.
Jonas J, Brissart H, Hossu G, Colnat-Coulbois S, Vignal J-P, Rossion B, Maillard L (2018) A face identity hallucination (palinopsia) generated by intracerebral stimulation of the face-selective right lateral fusiform cortex. Cortex 99:296–310.
Julian JB, Fedorenko E, Webster J, Kanwisher N (2012) An algorithmic method for functionally defining regions of interest in the ventral visual pathway. Neuroimage 60:2357–2364.
Kanwisher N, McDermott J, Chun MM (1997) The fusiform face area: a module in human extrastriate cortex specialized for face perception. J Neurosci 17:4302–4311.
Kanwisher N (2010) Functional specificity in the human brain: a window into the functional architecture of the mind. Proc Natl Acad Sci U S A 107: 11163–11170.
Kay KN, Weiner KS, Grill-Spector K (2015) Attention reduces spatial uncertainty in human ventral temporal cortex. Curr Biol 25:595–600.
Kietzmann TC, Swisher JD, König P, Tong F (2012) Prevalence of selectivity for mirror-symmetric views of faces in the ventral and dorsal visual pathways. J Neurosci 32:11763–11772.
Kriegeskorte N, Simmons WK, Bellgowan PSF, Baker CI (2009) Circular analysis in systems neuroscience: the dangers of double dipping. Nat Neurosci 12:535–540.
Kroenke CD, Bayly PV (2018) How forces fold the cerebral cortex. J Neurosci 38:767–775.
Kubota E, Grotheer M, Finzi D, Natu VS, Gomez J, Grill-Spector K (2023) White matter connections of high-level visual areas predict cytoarchitecture better than category-selectivity in childhood, but not adulthood. Cereb Cortex 33:2485–2506.
Kubota E, et al. (2025) White matter connections of human ventral temporal cortex are organized by cytoarchitecture, eccentricity and category-selectivity from birth. Nat Hum Behav 9:955–970.
Madan CR (2019) Robust estimation of sulcal morphology. Brain Inform 6:5.
McGugin RW, Gatenby JC, Gore JC, Gauthier I (2012) High-resolution imaging of expertise reveals reliable object selectivity in the fusiform face area related to perceptual performance. Proc Natl Acad Sci U S A 109:17063–17068.
McGugin RW, Newton AT, Gore JC, Gauthier I (2014) Robust expertise effects in right FFA. Neuropsychologia 63:135–144.
McGugin RW, Van Gulick AE, Tamber-Rosenau BJ, Ross DA, Gauthier I (2015) Expertise effects in face-selective areas are robust to clutter and diverted attention, but not to competition. Cereb Cortex 25:2610–2622.
McGugin RW, Van Gulick AE, Gauthier I (2016) Cortical thickness in fusiform face area predicts face and object recognition performance. J Cogn Neurosci 28:282–294.
McGugin RW, Newton AT, Tamber-Rosenau B, Tomarken A, Gauthier I (2020) Thickness of deep layers in the fusiform face area predicts face recognition. J Cogn Neurosci 32:1316–1329.
Mezer A, et al. (2013) Quantifying the local tissue volume and composition in individual brains with magnetic resonance imaging. Nat Med 19:1667–1672.
Miller JA, Voorhies WI, Lurie DJ, D'Esposito M, Weiner KS (2021) Overlooked tertiary sulci serve as a meso-scale link between microstructural and functional properties of human lateral prefrontal cortex. J Neurosci 41:2229–2244.
Mortazavi F, Romano SE, Rosene DL, Rockland KS (2017) A survey of white matter neurons at the gyral crowns and sulcal depths in the rhesus monkey. Front Neuroanat 11:69.
Natu VS, Barnett MA, Hartley J, Gomez J, Stigliani A, Grill-Spector K (2016) Development of neural sensitivity to face identity correlates with perceptual discriminability. J Neurosci 36:10893–10907.
Natu VS, et al. (2019) Apparent thinning of human visual cortex during childhood is associated with myelination. Proc Natl Acad Sci U S A 116:20750–20759.
Natu VS, Arcaro MJ, Barnett MA, Gomez J, Livingstone M, Grill-Spector K, Weiner KS (2021) Sulcal depth in the medial ventral temporal cortex predicts the location of a place-selective region in macaques, children, and adults. Cereb Cortex 31:48–61.
Nichols TE, Poline J-B (2009) Commentary on Vul et al.'s (2009) "puzzlingly high correlations in fMRI studies of emotion, personality, and social cognition". Perspect Psychol Sci 4:291–293.
Nordt M, Gomez J, Natu VS, Rezai AA, Finzi D, Kular H, Grill-Spector K (2021) Cortical recycling in high-level visual cortex during childhood development. Nat Hum Behav 5:1686–1697.
Norman-Haignere S, Kanwisher N, McDermott JH (2013) Cortical pitch regions in humans respond primarily to resolved harmonics and are located in specific tonotopic regions of anterior auditory cortex. J Neurosci 33:19451–19469.
Norman-Haignere SV, Albouy P, Caclin A, McDermott JH, Kanwisher NG, Tillmann B (2016) Pitch-responsive cortical regions in congenital amusia. J Neurosci 36:2986–2994.
Parker BJ, Voorhies WI, Jiahui G, Miller JA, Willbrand E, Hallock T, Furl N, Garrido L, Duchaine B, Weiner KS (2023) Hominoid-specific sulcal variability is related to face perception ability. Brain Struct Funct 228:677–685.
Parvizi J, Jacques C, Foster BL, Withoft N, Rangarajan V, Weiner KS, Grill-Spector K (2012) Electrical stimulation of human fusiform face-selective regions distorts face perception. J Neurosci 32:14915–14920.
Pinsk MA, Arcaro M, Weiner KS, Kalkus JF, Inati SJ, Gross CG, Kastner S (2009) Neural representations of faces and body parts in macaque and human cortex: a comparative FMRI study. J Neurophysiol 101:2581–2600.
Poldrack RA, Mumford JA (2009) Independence in ROI analysis: where is the voodoo? Soc Cogn Affect Neurosci 4:208–213.
Ramos Benitez J, Kannan S, Hastings WL, Parker BJ, Willbrand EH, Weiner KS (2024) Ventral temporal and posteromedial sulcal morphology in autism spectrum disorder. Neuropsychologia 195:108786.
Rangarajan V, Hermes D, Foster BL, Weiner KS, Jacques C, Grill-Spector K, Parvizi J (2014) Electrical stimulation of the left and right human fusiform gyrus causes different effects in conscious face perception. J Neurosci 34: 12828–12836.
Rosenke M, Davidenko N, Grill-Spector K, Weiner KS (2020) Combined neural tuning in human ventral temporal cortex resolves the perceptual ambiguity of morphed 2D images. Cereb Cortex 30:4882–4898.
Rosenke M, van Hoof R, van den Hurk J, Grill-Spector K, Goebel R (2021) A probabilistic functional atlas of human occipito-temporal visual cortex. Cereb Cortex 31:603–619.
Schalk G, Kapeller C, Guger C, Ogawa H, Hiroshima S, Lafer-Sousa R, Saygin ZM, Kamada K, Kanwisher N (2017) Facephenes and rainbows: causal evidence for functional and anatomical specificity of face and color processing in the human brain. Proc Natl Acad Sci U S A 114:12285–12290.
Scherf KS, Elbich DB, Motta-Mena NV (2017) Investigating the influence of biological sex on the behavioral and neural basis of face recognition. eNeuro 4:ENEURO.0104-17.2017.
Schrouff J, Raccah O, Baek S, Rangarajan V, Salehi S, Mourão-Miranda J, Helili Z, Daitch AL, Parvizi J (2020) Fast temporal dynamics and causal relevance of face processing in the human temporal cortex. Nat Commun 11:656.
Stigliani A, Weiner KS, Grill-Spector K (2015) Temporal processing capacity in high-level visual cortex is domain specific. J Neurosci 35: 12412–12424.
Stigliani A, Jeska B, Grill-Spector K (2019) Differential sustained and transient temporal processing across visual streams. PLoS Comput Biol 15: e1007011.
Susilo T, Duchaine B (2013) Advances in developmental prosopagnosia research. Curr Opin Neurobiol 23:423–429.
Thomas C, Avidan G, Humphreys K, Jung K-J, Gao F, Behrmann M (2009) Reduced structural connectivity in ventral visual cortex in congenital prosopagnosia. Nat Neurosci 12:29–31.
Tian X, Wang R, Zhao Y, Zhen Z, Song Y, Liu J (2020) Multi-item discriminability pattern to faces in developmental prosopagnosia reveals distinct mechanisms of face processing. Cereb Cortex 30:2986–2996.
Van Essen DC, et al. (2012) The human connectome project: a data acquisition perspective. Neuroimage 62:2222–2231.
Van Essen DC, Jbabdi S, Sotiropoulos SN, Chen C, Dikranian K, Coalson T, Harwell J, Behrens TEJ, Glasser MF (2014) Chapter 16: Mapping connections in humans and non-human primates: aspirations and challenges for diffusion imaging. In: *Diffusion MRI*, Ed 2. (Johansen-Berg H, Behrens TEJ, eds), pp 337–358. San Diego: Academic Press.

van Kooten IAJ, Palmen SJMC, von Cappeln P, Steinbusch HWM, Korr H, Heinsen H, Hof PR, van Engeland H, Schmitz C (2008) Neurons in the fusiform gyrus are fewer and smaller in autism. Brain 131:987–999.

Vul E, Harris C, Winkielman P, Pashler H (2009) Puzzlingly high correlations in fMRI studies of emotion, personality, and social cognition. Perspect Psychol Sci 4:274–290.

Weiner KS (2019) The mid-fusiform sulcus (sulcus sagittalis gyri fusiformis). Anat Rec 302:1491–1503.

Weiner KS, Grill-Spector K (2010) Sparsely-distributed organization of face and limb activations in human ventral temporal cortex. Neuroimage 52: 1559–1573.

Weiner KS, Grill-Spector K (2013) Neural representations of faces and limbs neighbor in human high-level visual cortex: evidence for a new organization principle. Psychol Res 77:74–97.

Weiner KS, Willbrand EH (2023) Is there an association between tuber involvement of the fusiform face area in autism diagnosis? Ann Neurol 93:1218–1220.

Weiner KS, Sayres R, Vinberg J, Grill-Spector K (2010) fMRI-adaptation and category selectivity in human ventral temporal cortex: regional differences across time scales. J Neurophysiol 103:3349–3365.

Weiner KS, Golarai G, Caspers J, Chuapoco MR, Mohlberg H, Zilles K, Amunts K, Grill-Spector K (2014) The mid-fusiform sulcus: a landmark identifying both cytoarchitectonic and functional divisions of human ventral temporal cortex. Neuroimage 84:453–465.

Weiner KS, et al. (2016) The face-processing network is resilient to focal resection of human visual cortex. J Neurosci 36:8425–8440.

Weiner KS, Barnett MA, Lorenz S, Caspers J, Stigliani A, Amunts K, Zilles K, Fischl B, Grill-Spector K (2017a) The cytoarchitecture of domain-specific regions in human high-level visual cortex. Cereb Cortex 27: 146–161.

Weiner KS, Yeatman JD, Wandell BA (2017b) The posterior arcuate fasciculus and the vertical occipital fasciculus. Cortex 97:274–276.

Weiner KS, et al. (2018) Defining the most probable location of the parahippocampal place area using cortex-based alignment and cross-validation. Neuroimage 170:373–384.

Willbrand EH, Ferrer E, Bunge SA, Weiner KS (2023) Development of human lateral prefrontal sulcal morphology and its relation to reasoning performance. J Neurosci 43:2552–2567.

Wilmer JB, Germine L, Chabris CF, Chatterjee G, Williams M, Loken E, Nakayama K, Duchaine B (2010) Human face recognition ability is specific and highly heritable. Proc Natl Acad Sci U S A 107:5238–5241.

Wilmer JB, Germine L, Chabris CF, Chatterjee G, Gerbasi M, Nakayama K (2012) Capturing specific abilities as a window into human individuality: the example of face recognition. Cogn Neuropsychol 29:360–392.

Witthoft N, Poltoratski S, Nguyen M, Golarai G, Liberman A, LaRocque KF, Smith ME, Grill-Spector K (2016) Reduced spatial integration in the ventral visual cortex underlies face recognition deficits in developmental prosopagnosia. bioRxiv:051102. Available at: https://www.biorxiv.org/content/10.1101/051102v1.full [Accessed January 31, 2023].

Zebrowitz L, Ward N, Boshyan J, Gutchess A, Hadjikhani N (2016) Dedifferentiated face processing in older adults is linked to lower resting state metabolic activity in fusiform face area. Brain Res 1644:22–31.

Zhang J, Liu J, Xu Y (2015) Neural decoding reveals impaired face configural processing in the right fusiform face area of individuals with developmental prosopagnosia. J Neurosci 35:1539–1548.

Zhang S, et al. (2022) Gyral peaks: novel gyral landmarks in developing macaque brains. Hum Brain Mapp 43:4540–4555.

Zhang S, et al. (2023) Species -shared and -unique gyral peaks on human and macaque brains. bioRxiv. Available at: http://dx.doi.org/10.1101/2023.07.26.550760

Zhao Y, Li J, Liu X, Song Y, Wang R, Yang Z, Liu J (2016) Altered spontaneous neural activity in the occipital face area reflects behavioral deficits in developmental prosopagnosia. Neuropsychologia 89:344–355.

Zhao Y, Zhen Z, Liu X, Song Y, Liu J (2018) The neural network for face recognition: insights from an fMRI study on developmental prosopagnosia. Neuroimage 169:151–161.

Zhen Z, Yang Z, Huang L, Kong X-Z, Wang X, Dang X, Huang Y, Song Y, Liu J (2015) Quantifying interindividual variability and asymmetry of face-selective regions: a probabilistic functional atlas. Neuroimage 113: 13–25.